

Is Geometry Enough for Matching in Visual Localization?

Qunjie Zhou^{1,*} Sérgio Agostinho^{2,*} Aljoša Ošep¹ Laura Leal-Taixé¹

¹Technical University of Munich ²Instituto Superior Técnico, Universidade de Lisboa, Portugal

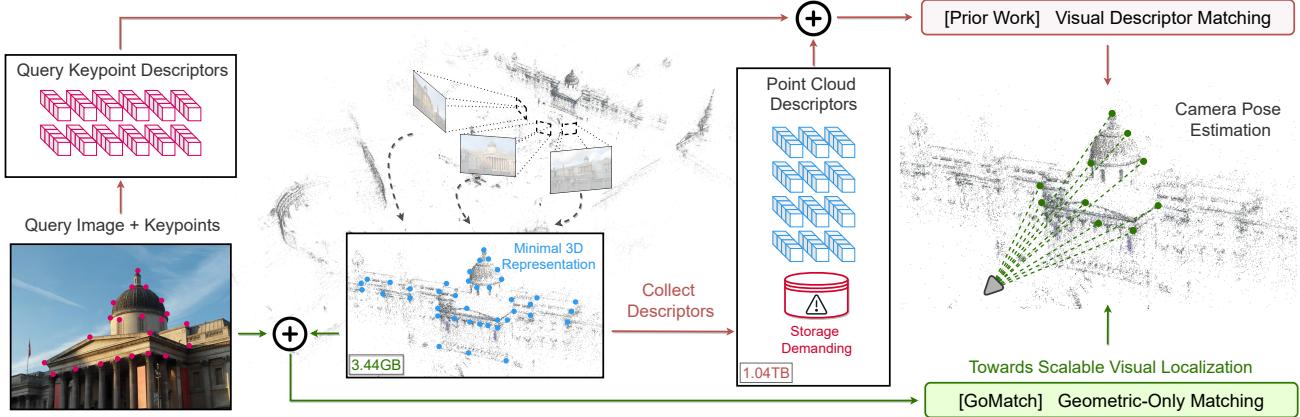


Figure 1. In this work, we propose GoMatch to tackle visual localization w.r.t. a scene represented as a 3D point cloud. By relying only on geometric information for matching, GoMatch allows structure-based methods to achieve localization solely through the use of keypoints, sidestepping the need to store visual descriptors for matching. Keeping only the minimal representation of a 3D model, *i.e.*, its coordinates, leads to a more scalable pipeline towards large-scale localization that bypasses privacy concerns and is easy to maintain.

Abstract

In this paper, we propose to go beyond the well-established approach to vision-based localization that relies on visual descriptor matching between a query image and a 3D point cloud. While matching keypoints via visual descriptors makes localization highly accurate, it has significant storage demands, raises privacy concerns and increases map maintenance complexity. To elegantly address those practical challenges for large-scale localization, we present GoMatch, an alternative to visual-based matching that solely relies on geometric information for matching image keypoints to maps, represented as sets of bearing vectors. Our novel bearing vectors representation of 3D points, significantly relieves the cross-domain challenge in geometric-based matching that prevented prior work to tackle localization in a realistic environment. With additional careful architecture design, GoMatch improves over prior geometric-based matching work with a reduction of (10.67m, 95.7°) and (1.43m, 34.7°) in average median pose errors on Cambridge Landmarks and 7-Scenes, while requiring as little as 1.5/1.7% of storage capacity in com-

parison to the best visual-based matching methods. This confirms its potential and feasibility for real-world localization and opens the door to future efforts in advancing city-scale visual localization methods that do not require storing visual descriptors.

1. Introduction

In this paper we tackle scalable, data-driven visual localization. The ability to localize a query image within a 3D map based representation of the environment is vital in many applications, ranging from robotics to virtual and augmented reality. In past years, researchers have made a significant progress in vision-based localisation [21, 16, 69, 40, 43, 48, 27, 72, 61, 51]. The majority of methods [64, 21, 69, 48, 61] rely on a pre-built 3D representation of the environment, typically obtained using structure-from-motion (SfM) techniques [54, 56]. Such 3D maps store 3D points and D -dimensional visual feature descriptors [52]. To determine the pose of a query image, *i.e.*, its 3D position and orientation, these methods match visual descriptors, obtained from the query image, with the ones stored in the point cloud. Once image-to-

*Equal contribution.

point-cloud matches are established, a Perspective-n-Point (PnP) solver [34, 24] is used to estimate the camera pose. While working well in practice, this approach suffers from several drawbacks. First, we need to explicitly store per-point visual descriptors for point clouds, which hinders its applicability to large-scale environments due to the expensive storage requirement. Second, this limits the applicability to point clouds with specific descriptors, which increases the 3D map maintenance effort – maps need to be re-built or updated to be used in conjunction with newly developed descriptors [20]. Third, this approach in practice necessitates a visual descriptor exchange between the server (storing the 3D model and descriptors) and an online feature extractor. This is a point of privacy vulnerability, as human identities and personal information can be recovered from visual descriptors intercepted during the transmission [44, 19, 18, 13, 22, 26, 59, 25].

The aforementioned issues lead to the main question we pose in this paper: *can we localize an image without relying on visual descriptors?* This would significantly reduce the map storage demands and simplify the map maintenance. Recently, Campbell *et al.* [9] showed that it is feasible to directly match 2D image keypoints with a 3D point cloud using only geometrical cues. However, this is limited to ideal scenarios where outliers are not present. This assumption does not hold in real-world scenes and is not directly applicable to challenging visual localization. This is not surprising, as relying only on geometrical cues is a significantly more challenging compared to matching visual descriptors. In contrast to a single 2D/3D point coordinate, a visual descriptor provides a rich visual context, since it is commonly extracted from the local image patch centered around a keypoint [21, 16, 69, 40].

In this paper, we achieve significant progress in making keypoints-to-point cloud direct matching ready for real-world visual localization. To cope with noisy images, point clouds, and inevitably keypoint outliers, we present **GoMatch**, a novel neural network architecture that relies on **Geometrical information only**. GoMatch leverages self- and cross-attention mechanisms to establish initial correspondences between image keypoints and point clouds, and further improves the matching robustness by filtering match outliers using a classifier. To the best of our knowledge, GoMatch is the first approach that is applicable to visual localization in the wild and does not rely on storage-demanding visual descriptors. In particular, compared to its prior work on geometric matching-based localization, GoMatch reduces the median pose errors (averaged across scenes) by (10.67m, 95.7°) and (1.43m, 34.7°) on Cambridge Landmarks dataset [32] and 7-Scenes dataset [57] confirming its potential in real-world visual localization.

We summarize our contributions as the following: (i) we develop a novel method to match query keypoints to a

point cloud relying only on geometrical information; (ii) We bridge the domain gap between a 2D image keypoint to a 3D point by projecting it into its co-visible reference views and show that this new representation is remarkably more robust compared to direct cross-domain matching; (iii) Our extensive evaluation shows that our method significantly outperforms prior work, effectively enabling real-world visual localization based on geometric-only matching; (iv) Finally, we thoroughly compare our method to the well-established visual localization baselines and discuss about the pros and cons for each approach. With this analysis, we hope to open the door for future progress towards more general and scalable structure-based methods for visual localization, which do not critically rely on storing visual descriptors, thereby reducing storage, map maintenance efforts, as well as privacy concerns.

2. Related Work

Structure-based localization. Structure-based localization methods [50, 47, 62, 55, 4] commonly establish explicit correspondences between the query image pixels and the 3D points of the environment to compute the query image pose from the established matches using PnP solvers [34, 24]. The keypoint correspondences are commonly established by computing and matching visual descriptors for each keypoint from a query and database images [21, 16, 69, 40, 27, 48, 61]. Another recent work [49] iteratively optimizes a camera pose by minimizing visual descriptor distances between the 3D points observed in the query and the reference images. While it does not establish matches, it relies on visual descriptors extracted from a neural network and requires 3D points. Structure-based localization methods achieve impressive localization accuracy and state-of-the-art performance [47, 16, 48] in the long-term localization benchmark [51, 64], containing extreme appearance changes and a high viewpoint variation. However, relying on visual descriptors [16, 21, 69, 40] makes the system demanding in storage¹, which limits the scalability of such methods. Several works [37, 11, 10, 41] propose to reduce the storage by scene compression, *i.e.*, selecting a subset of 3D points such that at least K points are seen from each database camera (so-called K-cover problem). In addition, [10] only keeps full descriptors for a minimal set of points to establish matches, and quantizes descriptors for other points using its nearest visual word in a learned vocabulary tree, as shown in [50]. While those methods can reduce storage requirements, they still suffer from the other two issues common to the use of visual descriptors in matching. For practical deployment of localization methods following a server-client model, we need to transmit visual

¹Storage as in non-volatile preservation of data, in contrast to volatile memory.

descriptors between the server and client, which exposes the model to a risk of a privacy breach [44, 19, 18, 13]. To mitigate the aforementioned issues, [20] focuses on how to efficiently update 3D models with newly-released descriptors and how to develop descriptors that are not vulnerable to privacy attacks [22]. In this paper, we propose an *orthogonal* direction to the aforementioned storage and privacy challenges in structure-based localization relying solely on more lightweight geometric information.

End-to-end learned localization. A recent trend of methods leverage data-driven techniques to learn to localize in an end-to-end manner, without relying on point clouds. This is achieved by either regressing scene coordinates, regressing the camera’s absolute pose or regressing its relative pose w.r.t. to a database image. Methods that directly regress dense 3D scene coordinates from the 2D images [4, 5, 7, 3, 12, 36, 71] do not require storing visual descriptors, however, they need to be re-trained for every new scene due to their lack of generalization [4, 5, 12, 6]. In certain cases, multiple instances of the same network are trained on sub-regions of the scene, due to the limited capacity of a single network [6]. Therefore, it is unclear how to scale these methods [4, 5, 7, 3, 12, 36, 71], that are traditionally evaluated only on small indoor rooms, to large-scale scenes. Absolute pose regression methods implicitly encode the scene representation inside the network and directly regress the pose from the query image [32, 30, 31, 46, 68]. However, such methods also require training a model per scene and have been shown to overfit to the viewpoints and appearance of the training images [53]. Another related approach that can sidestep maintaining a 3D model with visual descriptors, is to regress relative camera poses [17, 73, 2, 35] from a query image to its relevant database images. However, directly regressing the geometric transformations in general leads to limited generalization [53, 73]. Due to aforementioned issues we follow the path of explicit correspondence estimation between a query image to the 3D scene map, that does not require encoding scene-dependent information. We show in Section 5.6 that our method does generalize across scenes, requiring less storage and maintenance effort compared to the aforementioned methods.

Direct geometric keypoint matching. Matching image keypoints directly to 3D point clouds was first investigated in Campbell *et al.* [9]. Given a set of 2D keypoints in the query image and a set of 3D points in the scene point cloud, BPnPNet [9] jointly estimates matches between these two sets *purely* based on geometric information. However, this approach was shown to work in idealistic scenarios assuming no outlier keypoints and, as we experimentally demonstrate, the matching performance degrades significantly once outliers are introduced. The outlier-free as-

sumption clearly does not hold for challenging real-world localization scenarios as map building and keypoint detection are all challenging tasks, prone to errors and noise. In our work, we build upon BPnPNet [9] and design a geometric matching module that is robust against keypoint outliers. We show in Section 5.3 that our approach significantly outperforms BPnPNet in matching keypoints in presence of outliers, and thus making geometric-only matching for visual localisation feasible in practice.

3. Structure-based Localization

Overview. Structure-based methods assume as input a query image, a 3D point cloud of the scene, and database images with known poses. These methods first retrieve a set of database images that are co-visible with the query image, *i.e.*, have a visual overlap, as illustrated in Fig. 2. Next, after narrowing down the search space, they establish 2D-3D correspondences between the query image keypoints and a (retrieved) subset of the 3D point cloud. This set of correspondences can be used to estimate the query image pose using a PnP solver [29, 24]. The majority of prior work [21, 16, 69, 40, 27, 48, 47] rely on storage-consuming visual descriptors, stored together with the point cloud, to establish 2D-3D matches. The *key challenge* we address is how to establish those correspondences *without* visual descriptors.

Notations. We assume two point sets, one with 2D keypoint coordinates in the image plane $\mathbf{p}_i \in \mathbb{R}^2$, and the second containing 3D point coordinates $\mathbf{q}_j \in \mathbb{R}^3$. We seek the matching set $\mathcal{M} := \{(i, j) | \mathbf{p}_i = \pi(\mathbf{q}_j; \mathbf{K}, \mathbf{R}, \mathbf{t})\}$, *i.e.*, the set of index pairs i and j , for which if the j -th 3D keypoint is projected to the image plane, it matches the coordinates specified by the corresponding i -th 2D point. The camera intrinsic matrix $\mathbf{K} \in \mathbb{R}^{3 \times 3}$ is assumed to be known, and the operator $\pi(\cdot)$ represents the camera projection function, which transforms 3D points onto the camera’s frame of reference and projects them to the image plane according to the camera’s intrinsics. Our goal is to find the correct 2D-3D keypoint matches for accurate pose estimation.

Keypoint representation. We represent 2D pixels using 2D coordinates $(u, v) \in \mathbb{R}^2$ in the image plane. To learn a matching function that is agnostic to different camera models, we uplift those 2D points into a bearing vector representation $\mathbf{b} \in \mathbb{R}^2$, effectively removing the effect of the camera intrinsics. Bearing vectors encode the direction (or bearing) of points in a camera’s frame of reference. We compute bearing vectors from image pixels as: $[\mathbf{b}^\top 1]^\top = \mathbf{K}^{-1}[u \ v \ 1]^\top$. For a 3D point, we consider two different representations (see Fig. 2): (i) as 3D coordinates $(x, y, z) \in \mathbb{R}^3$ w.r.t. a 3D world reference/origin; and (ii) as a bearing vector w.r.t. a reference database image. The bearing vector representation allows bringing both 2D pix-

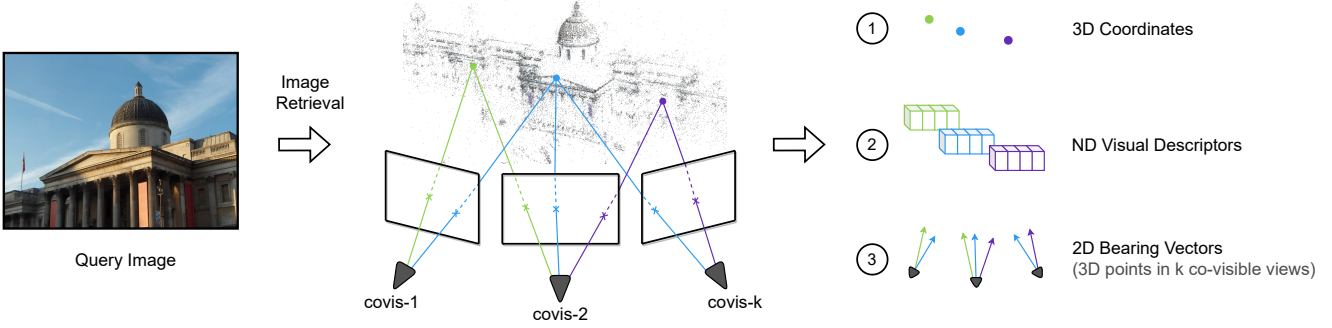


Figure 2. Co-visible views & keypoint representations. Retrieving co-visible reference images (views) of a query image narrows the matching against a full 3D point cloud to a subset of points that are more likely to be visible to the query image. Each 3D point can be represented differently by: 1) its 3D coordinate; 2) a visual descriptor that incorporates local appearance; or 3) a bearing vector that represents the direction from the reference camera origin to a 3D point in normalized coordinates. In this paper, we explore keypoint matching using representations 1) and 3).

els and 3D points to the same data modality. Given a 3D point $\mathbf{p} \in \mathbb{R}^3$ and transformation (\mathbf{R}, \mathbf{t}) from the world to the database image’s frame of reference, we compute the corresponding the bearing vector as:

$$\mathbf{p}' = \mathbf{R}\mathbf{p} + \mathbf{t}, [\mathbf{b}^\top 1]^\top = \mathbf{p}'/p'_z, \quad (1)$$

where \mathbf{p}' represents \mathbf{p} in the camera’s frame of reference, and p'_z represents its z coordinate. As shown in Table 2, these geometric-based point representations requires significantly lower storage compared to visual descriptor based ones, *e.g.*, as low as 3% compared to the storage of modern descriptors.

4. Geometric-only Matching

BPnNet in a Nutshell. To the best of our knowledge, BPnNet [9] is the first step towards establishing correspondence between the query keypoints and 3D point cloud in the absence of visual descriptors. It proposes an end-to-end trainable, differentiable matcher that performs 2D to 3D cross domain matching without relying on appearance information. While this is a step in the right direction, we show in Section 5.3 that it does not transfer to real-world visual localization scenarios where outliers, *i.e.*, points without a match, are pervasive. Direct 2D-3D matching of sparse keypoints is a challenging problem due to low amount of discriminative data, *i.e.*, points no longer have a local visual appearance, and its cross-domain nature. In a nutshell, BPnNet (i) encodes points to obtain per point features, (ii) establishes matches using the Sinkhorn algorithm [14, 58], which finds the optimal assignment between geometrical features, and finally, (iii) leverages a differentiable PnP solver that imposes an additional pose supervision on the network. In the following, we build on the observation that the lightweight geometric feature encoder does not possess the necessary representational power to produce

features that generalize simultaneously to situations with and without outliers.

4.1. GoMatch: Embracing Outliers

In GoMatch we (i) propose architectural changes that enable resilience to outliers and (ii) cast the *cross-domain* nature of 2D-3D matching to an *intra-domain* setting through the use of bearing vectors. Below, we explain the details of these contributions, which are experimentally validated to be all necessary and critical to outlier-robust geometric matching in Section 5.3. We refer to Fig. 3 for a visual overview of the entire network. Furthermore, we add an outlier rejection layer to retain only quality matches from the Sinkhorn outputs. While we introduce the novel network components in the following paragraphs, we refer the reader to the supplementary material for an in-depth description of all network components.

Feature refinement through attention. In BPnNet, each keypoint node is processed in parallel with an MLP-style encoder to extract features directly for matching, and information exchange happens only in the Sinkhorn matching stage. This might lead to a learned feature representation which lacks context information within each 2D/3D domain and cross domains. Based on this assumption, we explore adding information exchange prior to matching. To enhance the context information within each domain, we apply *self-attention* to the raw encoded features where a graph neural network [28] refines features of every keypoint by exchanging the information with a fixed number of closest neighbors in coordinate space. This is followed by *cross-attention* [67], where every keypoint from one domain will interact with all keypoints from the other domain through a sequence of multi-head attention layers. By stacking several blocks of such self-/cross-attention layers, we are able to learn more representative features, for significantly more accurate matching.

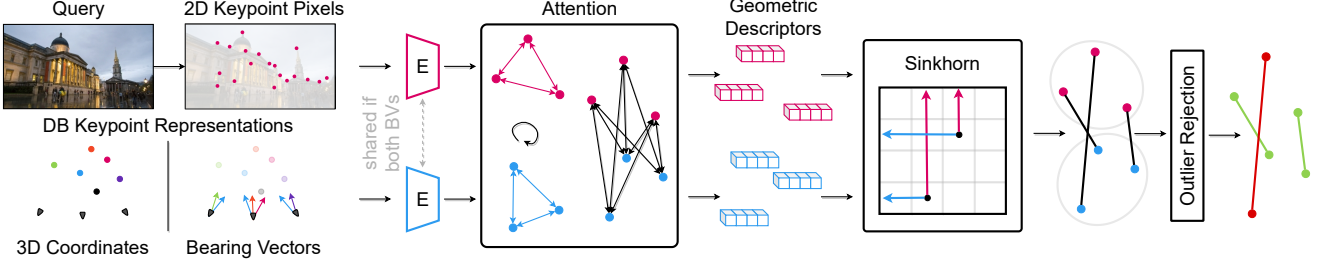


Figure 3. GoMatch components overview. The query image and database keypoints first undergo a feature encoder E to generate per-point features. We share encoders in the query and database branch when database points are represented as bearing vectors otherwise not. These features are refined in the attention layer and then used in the Sinkhorn matching stage to establish an initial set of candidate matches, from which erroneous matches are filtered with an outlier rejection layer.

Outlier rejection. After Sinkhorn matching, the estimated corresponding pairs may still contain outlier matches. To filter those further, we follow [42] and add a classifier that takes in the concatenated geometric features from the query and database keypoints, and predicts confidence scores for all matches. Estimated correspondences with confidence below a threshold (0.5 in practice) are rejected.

Matching with bearing vectors. Directly matching 2D keypoints to cross-domain 3D coordinates is challenging because it requires the network to learn features that have to consider not only the relationship between keypoints, but also the influence of different camera poses. Furthermore, the different distributions of 3D point clouds between datasets, *e.g.*, different scene sizes or different gravity directions, are particularly challenging for a single encoder to learn. Based on this observation, we propose to leverage the *bearing vector* representation of the database points to reduce the domain gap. Intuitively, this representation disentangles the influence of the camera pose by projecting 3D points onto the normalized image plane, which also avoids encoding information about individual camera intrinsic parameters. Finally, bearing vectors provide a common domain between query and database keypoints, eliminating the need for a separate encoder. As we demonstrate in our experimental section, the change in input type has a substantial positive effect.

4.2. Training GoMatch

All of our models are trained to learn feature matching and outlier filtering jointly, using a matching loss and an outlier rejection loss.

Matching Loss. The Sinkhorn matching layer is trained to output a discrete joint probability distribution of two sets of keypoints being matched. We denote this distribution as $\tilde{P} \in \mathbb{R}_+^{M+1 \times N+1}$, such that $\sum_{i=1}^{M+1} \sum_{j=1}^{N+1} \tilde{P}_{ij} = 1$, *i.e.*, is a valid probability distribution. Here, M and N denote the total number of query and database keypoints considered during the matching. We include an extra row and column

to allow keypoints not to be matched. We employ a negative log loss to the joint discrete probability distribution. Consider the set of all ground truth matches \mathcal{M} , as well as the set of unmatched query keypoints \mathcal{U}_q and database keypoints \mathcal{U}_d . The matching loss is of the form:

$$L_{\text{match}} = -\frac{1}{N_m} \sum_{(i,j) \in \mathcal{M}} \log \tilde{P}_{ij} - \frac{1}{N_m} \sum_{i \in \mathcal{U}_q} \log \tilde{P}_{i(N+1)} - \frac{1}{N_m} \sum_{j \in \mathcal{U}_d} \log \tilde{P}_{(M+1)j}, \quad (2)$$

where $N_m = |\mathcal{M}| + |\mathcal{U}_q| + |\mathcal{U}_d|$.

Outlier Rejection Loss. For the outlier rejection layer we employ a mean weighted binary cross-entropy loss:

$$L_{\text{or}} = -\frac{1}{N_c} \sum_{i=1}^{N_c} w_i (y_i \log p_i + (1 - y_i) \log(1 - p_i)), \quad (3)$$

where N_c denotes the total number of correspondences supplied to the outlier rejection layer. The term p_i denotes the classifier output probability for each correspondence, while y_i denotes the correspondence target label, and w_i is the weight balancing the negative and positive samples. Our final loss balances both terms equally, *i.e.*, $L_{\text{total}} = L_{\text{match}} + L_{\text{or}}$. We present implementation details about training and testing process in our supplementary material.

5. Experimental Evaluation

In this section, we thoroughly study the potential of using our proposed geometric-based matching for the task of real-world visual localization. We start our experiments by testing the robustness of BPnNet [9] and GoMatch with keypoint outliers. Next, we verify our technical contribution of successfully diagnosing the missing components leading to robust geometric matching and enabling geometry-based visual localization. Furthermore, we position geometric-based localization among other state-of-the-art visual localization approaches by comprehensively analysing each

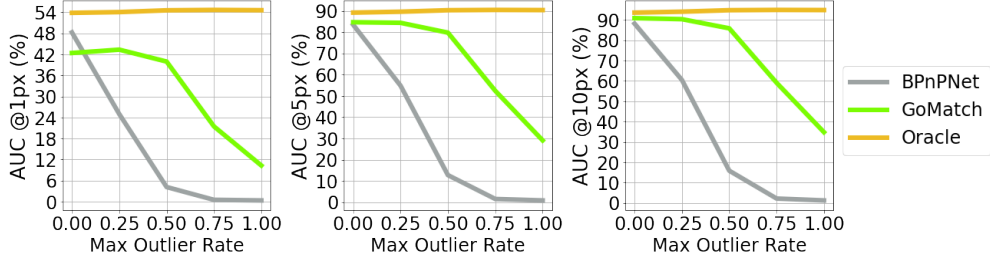


Figure 4. Influence of keypoint outlier rate. In contrast to prior work BPNPnet [9], GoMatch is significantly more robust against keypoint outliers thanks to the more powerful attention-based architecture as well as our novel formulation of matching same-domain bearing vectors instead of cross-domain features.

method in terms of localization accuracy, maintenance effort, privacy risk, and storage demands (Section 5.5). Finally, we present a generalization study (Section 5.6) to highlight that our proposed method generalizes across different types of datasets and keypoint detectors. We hope that our in-depth study serves as a starting point of this rarely explored new direction, and inspires new work to advance scalable visual localization through geometric-only matching in the future.

5.1. Datasets

We use **MegaDepth** [38] for training and ablation given its large scale. It consists of images captured in-the-wild from 196 outdoor landmarks. We adopt the original test set proposed in [38], and split the remaining sequences into training and validation sets. After verifying our best models on MegaDepth, we evaluate them on the popular Cambridge Landmarks [32] (Cambridge) dataset which consists of 4 outdoor scenes with varying scales. It allows convenient comparison to other localization approaches. We use the 3D scene point cloud released by [49]. In addition, we evaluate on the indoor **7-Scenes** [57] dataset to further assess the generalization capability of our method. 7-Scenes is composed of dense point clouds captured by an RGB-D sensor, and thus provides an alternative environment with different keypoint distributions, in both 2D images and 3D point clouds. We perform evaluation on the official test splits released by the Cambridge and 7-Scenes datasets. We provide detailed information about training data generation using MegaDepth in the supplementary.

5.2. Experimental Setup

Keypoint detection. For MegaDepth and Cambridge, we use respectively SIFT [39] and SuperPoint [16], *i.e.*, the same keypoint detector used to obtain the 3D scene models. For 7-Scenes, we are allowed to apply different detectors, *i.e.*, both SIFT and SuperPoint, to extract keypoints using the depth maps provided by the dataset.

Retrieval pairs. We use ground truth to sample retrieval pairs that have at least 35% visual overlapping in

MegaDepth to ensure enough matches are present during training, as well as to isolate the side-effect of retrieval performance during ablations. For evaluation and comparison to state-of-the-art localization methods, we follow [49] and use their *top-10* pairs retrieved using NetVLAD [1] on Cambridge and DenseVLAD [65] on 7-Scenes.

Matching baselines. We consider BPNPNet [9] as our geometric-based matching baseline. For a fair comparison, we re-train BPNPNet using our training data. Our visual-based matching baselines use SIFT [39], CAPS [69] and SuperPoint [16] as keypoint descriptors. To match visual descriptors, we use the commonly adopted nearest neighbor search [43] with mutual consistency check.

Localization pipeline. We use the structure-based localization pipeline introduced in Section 3, where we first obtain up to $k = 10$ retrieval pairs between a query and database images. Then we establish per-pair 2D to 3D matches using either a geometric-based or a visual-based matching model, and then merge results from k pairs based on their matching scores to estimate camera poses. For fairness, all matching baselines use identical retrieval pairs and identical settings for the PnP+RANSAC solver [29].

Evaluation metrics. For MegaDepth, we follow BPNPNet [9] and report the pose error quantiles at 25/50/75% for the translation and rotation ($^{\circ}$) errors as evaluation metrics. However, as the scale unit of MegaDepth is undetermined and varies between scenes, the translation errors are not consistent between scenes. Therefore, we propose a new metric based on pixel-level reprojection errors that preserves scene consistency. For each query, we project its inlier 3D keypoints using the predicted and the ground-truth poses. We then report the area under the cumulative curve (AUC) of the mean reprojection error up to 1/5/10px, inspired by the pose error based AUC metric used in [60, 49]. We report the commonly used median translation (m) and rotation ($^{\circ}$) errors [32, 53, 10] per-scene on Cambridge and 7Scenes.

Model	3D Repr.	Share Encoder	Att	OR	Rotation (°) Quantile@25/50/75% (↓)	Translation	Reproj. AUC (%) @1/5/10px (↑)
Oracle					0.03/0.06/0.10	0.00/0.00/0.01	54.58/90.37/94.87
BPnPNet	Coords	✗	✗	✗	15.17/31.05/59.78	1.67/3.14/5.31	0.34/0.83/1.21
BPnPNet ($k = 10$)	Coords	✗	✗	✗	16.03/33.27/63.90	1.59/3.24/5.80	0.56/1.08/1.50
Variants	BVs	✗	✗	✗	12.19/27.68/58.22	1.26/2.8/5.14	0.37/1.48/2.18
	BVs	✓	✗	✗	9.16/22.62/53.20	0.98/2.38/4.72	0.85/3.09/4.36
	BVs	✓	✓	✗	0.55/8.08/29.34	0.05/0.84/3.34	9.13/25.71/31.65
	BVs	✗	✓	✓	0.38/7.46/31.75	0.04/0.83/3.73	10.22/28.17/33.69
	Coords	✗	✓	✓	4.09/23.56/63.21	0.37/2.53/5.93	3.81/13.54/17.46
GoMatch	BVs	✓	✓	✓	0.36/6.97/29.85	0.03/0.69/3.38	10.30/29.08/34.79
GoMatch($k = 10$)	BVs	✓	✓	✓	0.15/0.95/13.00	0.01/0.09/1.55	15.14/42.39/51.24

Table 1. GoMatch ablation. *Top*: We present Oracle for reference and re-trained BPnPNet [9] as our baseline. *Middle*: We study how the 3D representation (Repr.) and architectural changes influences the performance. Using bearing vector (BVs) instead of 3D coordinates (Coords) as representation and introducing feature attention (Att) are the most crucial factors to the performance improvement. Together with further benefits from the outlier rejection (OR) component and sharing the query and database keypoint feature encoders leads us to the full GoMatch model (*Bottom*). All results rely on a single retrieval image unless stated otherwise, *e.g.*, $k = 10$.

5.3. Ablations

We perform ablation studies with MegaDepth’s [38] test split, where all retrieval pairs have guaranteed 35% co-visibility, to focus purely on matching performance. In addition, we study the effect of using a single co-visible reference view ($k = 1$) as a minimal setting, as well as multiple views, *e.g.*, $k = 10$, following the common practice in hierarchical structure-based localization [49, 53]. To better understand the new AUC metric, we also present an **Oracle** that uses ground truth matches as its prediction. It is used to show the upper-bound performance that can be achieved using our metric and generated data.

Sensitivity to keypoint outliers. In a real-world localization setting, the detected query image keypoints will often be noisy and will not have a direct correspondence in the 3D point cloud. Keypoint matching methods thus need to be able to cope with outliers. We first study whether our baseline has this capability by manually increasing the maximum outlier rate, ranging from 0 to 1. The outlier rate is computed as the number of ground-truth (gt) correspondences divided by the total number of 2D or 3D keypoints. For all other experiments, we will not control keypoint the outlier rate to properly mimic realistic conditions. As shown in Fig. 4, the Oracle stays round 55/90/94% (AUC@1/5/10px). The large error at 1px is due to our match generation process that admits a 1px error threshold (*c.f.* supplementary for a detailed discussion). BPnPNet [9] slightly outperforms GoMatch at 1px threshold, being similarly accurate to us at 5/10px thresholds in the absence of outliers. However, as the ratio of outliers increases, the performance of BPnPNet drastically drops, while GoMatch gracefully handles outliers, *i.e.*, GoMatch is always above 80% at 5/10px up to 50% of outliers. This experiment con-

firms that GoMatch is significantly more robust to outliers compared to BPnPNet. This outlier robustness is achieved through careful modifications to the network architecture and 3D point representation, both validated by a thorough performance analysis presented in the next sections.

Architecture-level analysis. In Table 1 (*Top*), we present the Oracle and BPnPNet [9] re-trained on our data for a direct comparison with GoMatch. This is paired with additional variants, progressively transitioning from BPnPNet to GoMatch. We found that shared encoding brings performance gains up to 0.48/1.61/2.18 AUC percentage points. Adding feature attention on top leads to a significant improvement of 8.28/22.62/27.29 AUC percentage points. By further adding the outlier rejection increases the AUC by 1.17/3.37/3.14 percentage points. We conclude that these network components yield 9.93/27.6/32.61 percentage points of improvements in terms of AUC scores when using bearing vectors the representation.

Representation-level analysis. Table 1 also shows that using 3D coordinates (Coords) instead of bearing vectors (BVs), even with attention and outlier rejection, hinders performance dramatically by 6.49/15.54/17.33 percentage points. If we only change the representation from Coords to BVs, without attention nor outlier rejection, the improvement is merely 0.31/1.29/1.9 percentage points. Therefore, we verify the bearing vector representation is as important as the architectural changes, and both contribute towards keypoint outlier resilience. By modifying both architecture and representation, GoMatch outperforms the re-trained BPnPNet by 9.96/28.25/33.58 AUC percentage points.

Utilizing multiple co-visible images. As shown in Table 1, when using $k = 10$ co-visible views, both methods

	Method	Easy Maintenance	Privacy	Database Storage (GB, ↓)				Total
				Cameras (MB)	3D	Raw Imgs	Descs	
VM	SIFT [39]	✗	✗	15.73	3.44	✗	130.10 (uint8)	133.33
	CAPS [69]	✗	✗	15.73	3.44	✗	520.38 (fp32)	523.83
	SuperPoint [16]	✗	✗	15.73	3.44	✗	1040.76 (fp32)	1044.21
	Extract on-the-fly	✗	✗	15.73	3.44	157.84	✗	161.29
GM	BPnNet [9]	✓	✓	15.73	3.44	✗	✗	3.45
	GoMatch	✓	✓					

Table 2. On the challenges of large-scale structure-based localization. We compare visual-based matching (VM) and geometric-based matching (GM) methods and analyse whether a method is easily maintained and provides privacy protection and analysing their storage required for large-scale localization. We show using GM instead of VM, significantly reducing storage demands for localization while simultaneously safeguarding user privacy and require effortless maintenance.

improved their result: BPnNet by a small margin and GoMatch by a large margin of 4.84/13.31/16.45 AUC percentage points. We thus use $k = 10$ for all of the following experiments.

5.4. Practical Challenges in Large-scale Localization

As introduced in Section 1 and Section 2, the primary motivation of our work is to present a new localization framework that does not suffer from: (i) storage requirements, (ii) maintenance effort, and (iii) privacy concerns. These are challenges that current structure-based localization methods face, especially when it comes to scaling-up for city-level scenes. A considerable amount of literature focuses on making localization methods more accurate, however, those practical challenges are much less explored. To study the storage requirement, we perform a detailed analysis on MegaDepth, which resembles a city-level large-scale environment. While MegaDepth is a collection of landmarks instead of a real city-scale scene, we argue that a city-scale scene consists of a collection of districts (similar to landmarks). As shown in Table 2, the minimal scene data, *i.e.*, scene coordinates (3D) and camera metadata (Cameras), is always required by a structured-based localization to obtain 2D-3D correspondences, which will take 15.73MB and 3.44GB storage in total for all Megadepth scenes. This is the only data that geometric-based matching (GM) methods need to store. This is in contrast to visual-based matching (VM) as they need to store extra visual descriptors that consume 130/520/1040GB for SIFT/CAPS/SuperPoint descriptors (descriptor dimensions are 128/256/256). Alternatively, one can extract descriptors on-the-fly from the retrieved raw images, which requires saving all of the raw images with an extra storage of 157GB and leading to more computational burden. **Then**, after addressing the storage issue, one still needs to consider the privacy concern raised during descriptor transmission, since large-scale localization with a 3D map has to be realistically deployed in a server-client mode, where sever stores the 3D

scene data required to perform localization. This is another motivation driving us towards using geometric information only. **Finally**, as thoroughly covered in [20], with continuous advance on local features, upgrading descriptors is inevitable in the long-term, which involves either re-building the map or transforming the descriptors. In contrast, for geometric-based matching, upgrading our localization algorithm does not need an update on the map side (unless the scene has changed, in which case any map would need to be updated).

5.5. Comparison to localization Baselines

Following the discussion in Section 5.4, we comprehensively compare GoMatch with other established baselines by looking beyond localization performance, and considering as well the storage footprint, resiliency to privacy attacks, and ease of maintenance. As shown in Table 3, DSAC++ is the most accurate method while being resilient to privacy attacks as it does not need to transmit visual descriptors. However, as it requires 4 models (each trained per-scene), it requires 828 MB storage to work under 4 scenes compared to our 48.12 MB. Note, for MegaDepth, this would imply re-training and deploying 196 models which occupy ~ 40 GB storage compared to our 3.5 GB. The only method being more storage-efficient than GoMatch is hybrid scene compression (HybridSC) as it keeps only 1.5% if its original points via compression. However, it is unclear whether the privacy issue still remains for this method since it still relies on full visual descriptors to perform matching. In addition to the maintenance effort involved in upgrading descriptors as all VM methods do, HybridSC requires extra effort to re-compress the scenes once its geometry gets updated. On the whole, GoMatch properly balances those three aspects showing benefits in storage, ease of maintenance, and privacy and meanwhile achieves performance on par with PoseNet. Compared to its visual-descriptor SuperPoint counterpart, GoMatch requires only 1.5% of the capacity to store same scene. GoMatch reduces the average pose errors by $(10.67m, 95.7^\circ)$ compared to our

	Method	Storage (MB)	Easy Maintenance	Privacy	King's College	Old Hospital Median Pose Error (m, °) (↓)	Shop Facade	St. Mary's Church
E2E	PoseNet [32]	200	✗	✓	1.92/5.40	2.31/5.38	1.46/8.08	2.65/8.48
	DSAC++ [5]	828	✗	✓	0.18/0.30	0.20/0.30	0.06/0.30	0.13/0.40
VM	HybridSC [10]	3.13	✗	?	0.81/0.59	0.75/1.01	0.19/0.54	0.50/0.49
	Active Search [50]	812.7	✗	✗	0.42/0.55	0.44/1.01	0.12/0.40	0.19/0.54
	SuperPoint [16]	3214.84	✗	✗	0.16/0.38	0.33/1.04	0.07/0.54	0.16/0.54
GM	BPnPNet [9]	48.15	✓	✓	26.73/106.99	24.8/162.99	7.53/107.17	11.11/49.74
	GoMatch	48.15	✓	✓	0.25/0.64	2.83/8.14	0.48/4.77	3.35/9.94

Table 3. Comparison to existing localization baselines. We consider end-to-end (E2E) methods and structure-based methods that either matches visual descriptors (VM) or geometries (GM). *Easy Maintenance* is checked if a method does not require re-caching the descriptors for upgrading the algorithm or retraining the model when the map geometry is updated.

	Method	Storage (MB)	Easy Main.	Priv -acy	Chess	Fire	Heads	Office	Pumpkin	Kitchen	Stairs
E2E	PoseNet [32]	350	✗	✓	0.32/8.12	0.47/14.4	0.29/12.0	0.48/7.68	0.47/8.42	0.59/8.64	0.47/13.8
	DSAC++ [5]	1449	✗	✓	0.02/0.50	0.02/0.90	0.01/0.80	0.03/0.70	0.04/1.10	0.04/1.10	0.09/2.60
VM	Active Search [50]	-	✗	✗	0.04/1.96	0.03/1.53	0.02/1.45	0.09/3.61	0.08/3.10	0.07/3.37	0.03/2.22
	SIFT [39]	2923	✗	✗	0.03/1.13	0.03/1.08	0.02/2.19	0.05/1.42	0.07/1.80	0.06/1.84	0.18/4.41
	SuperPoint [16]	22977	✗	✗	0.03/1.28	0.03/1.3	0.02/1.99	0.04/1.31	0.06/1.63	0.06/1.73	0.07/1.91
GM	BPnPNet [9](SIFT)	302	✓	✓	1.29/43.82	1.48/51.82	0.93/55.13	2.61/59.06	2.15/39.85	2.15/43.00	2.98/60.27
	BPnPNet (SuperPoint)	397	✓	✓	1.25/43.9	1.42/45.09	0.8/50.05	2.33/14.54	1.71/31.81	1.68/33.91	2.1/55.78
	GoMatch (SIFT)	302	✓	✓	0.04/1.65	0.13/3.86	0.09/5.17	0.11/2.48	0.16/3.32	0.13/2.84	0.89/21.12
	GoMatch (SuperPoint)	397	✓	✓	0.04/1.56	0.12/3.71	0.05/3.43	0.07/1.76	0.28/5.65	0.14/3.03	0.58/13.12

Table 4. Generalization study on 7-Scenes. GoMatch generalizes between different scene types and detector types and outperforming BPnPNet and PoseNet.

only prior geometric-based matching work, significantly reducing the accuracy gap to state-of-the-art methods. We hope this inspires researchers to pursue this line of work.

5.6. Generalization

As our final experiment, we study the generalization capability of our method in terms of localization in different types of scenes, *e.g.*, indoor and outdoor, and matching keypoints obtained using different detectors. According to our results in Table 4, similar to our previous experiments, we outperform BPnPNet by a large margin achieving (1.43m, 34.7°) lower average median pose errors. Except for GoMatch with SIFT keypoints which produces a relatively large 21.12° median rotation error in Stairs, we are only slightly worse than our visual-based matching baselines with SIFT and SuperPoint. Yet, we require only 10/1.7% of the storage that is required by SIFT/SuperPoint to store maps. We also largely outperform PoseNet [32] in all metrics for all scenes except for the relatively lower translation error in Stairs scene, *i.e.*, (0.47m vs 0.58m). The results clearly verify that GoMatch trained on outdoor scenes (MegaDepth) generalizes smoothly to indoor scenes (7-Scenes), being agnostic to scene types. Similarly, we also confirm that GoMatch trained with SIFT keypoints

generalizes well to SuperPoint keypoints, being agnostic to detector types.

6. Conclusion

We present GoMatch, a novel sparse keypoint matching method for visual localization that relies only on geometrical information and that carefully balances common practical challenges of large-scale localization, namely: localization performance, storage demands, privacy and ease of maintenance. From all these, the last three are often overlooked. Through a rigorous architecture design process, GoMatch dramatically surpasses its prior work in handling outliers, enabling it for real-world localization. Compared to localization pipelines using visual descriptor-based matching, GoMatch allows localization with a minimal 3D scene representation, requiring as little as 1.5/1.7% to store the same scene. Geometric-based matching brings localization pipelines to a new level of scalability that opens the door for localizing in much larger environments. We see our work as a starting point for this new direction and we look forward to inspire other researchers to pursue more accurate and reliable geometric-based visual localization in the future.

References

- [1] Relja Arandjelovic, Petr Gronat, Akihiko Torii, Tomas Pajdla, and Josef Sivic. Netvlad: Cnn architecture for weakly supervised place recognition. In *IEEE Conf. Comput. Vis. Pattern Recog.*, 2016. 6, 14, 15
- [2] Vassileios Balntas, Shuda Li, and Victor Prisacariu. Relocnet: Continuous metric learning relocalisation using neural nets. In *Eur. Conf. Comput. Vis.*, September 2018. 3
- [3] Aritra Bhowmik, Stefan Gumhold, Carsten Rother, and Eric Brachmann. Reinforced feature points: Optimizing feature detection and description for a high-level task. In *IEEE Conf. Comput. Vis. Pattern Recog.*, pages 4948–4957, 2020. 3
- [4] Eric Brachmann, Alexander Krull, Sebastian Nowozin, Jamie Shotton, Frank Michel, Stefan Gumhold, and Carsten Rother. DSAC - Differentiable RANSAC for Camera Localization. In *IEEE Conf. Comput. Vis. Pattern Recog.*, 2017. 2, 3
- [5] Eric Brachmann and Carsten Rother. Learning less is more - 6d camera localization via 3d surface regression. In *IEEE Conf. Comput. Vis. Pattern Recog.*, 2018. 3, 9
- [6] Eric Brachmann and Carsten Rother. Expert sample consensus applied to camera re-localization. In *IEEE Conf. Comput. Vis. Pattern Recog.*, pages 7525–7534, 2019. 3
- [7] Eric Brachmann and Carsten Rother. Neural-guided ransac: Learning where to sample model hypotheses. In *Int. Conf. Comput. Vis.*, pages 4322–4331, 2019. 3
- [8] G. Bradski. The OpenCV Library. *Dr. Dobbs's Journal of Software Tools*, 2000. 16
- [9] Dylan Campbell, Liu Liu, and Stephen Gould. Solving the blind perspective-n-point problem end-to-end with robust differentiable geometric optimization. In *Eur. Conf. Comput. Vis.*, pages 244–261. Springer, 2020. 2, 3, 4, 5, 6, 7, 8, 9, 13, 16
- [10] Federico Camposeco, Andrea Cohen, Marc Pollefeys, and Torsten Sattler. Hybrid scene compression for visual localization. In *Proceedings of the IEEE/CVF Conference on Computer Vision and Pattern Recognition (CVPR)*, June 2019. 2, 6, 9
- [11] Song Cao and Noah Snavely. Minimal scene descriptions from structure from motion models. In *Proceedings of the IEEE Conference on Computer Vision and Pattern Recognition (CVPR)*, June 2014. 2
- [12] Tommaso Cavallari, Luca Bertinetto, Jishnu Mukhoti, Philip Torr, and Stuart Golodetz. Let’s take this online: Adapting scene coordinate regression network predictions for online rgb-d camera relocalisation. In *3DV*, pages 564–573. IEEE, 2019. 3
- [13] Kunal Chelani, Fredrik Kahl, and Torsten Sattler. How privacy-preserving are line clouds? recovering scene details from 3d lines. In *IEEE Conf. Comput. Vis. Pattern Recog.*, pages 15668–15678, 2021. 2, 3
- [14] Marco Cuturi. Sinkhorn distances: Lightspeed computation of optimal transport. In *NeurIPS*, pages 2292–2300, 2013. 4, 13, 14
- [15] Haowen Deng, Tolga Birdal, and Slobodan Ilic. Ppfnet: Global context aware local features for robust 3d point matching. In *Proceedings of the IEEE Conference on Computer Vision and Pattern Recognition (CVPR)*, June 2018. 15
- [16] Daniel DeTone, Tomasz Malisiewicz, and Andrew Rabinovich. Superpoint: Self-supervised interest point detection and description. In *CVPR Workshops*, pages 224–236, 2018. 1, 2, 3, 6, 8, 9, 15, 16
- [17] Mingyu Ding, Zhe Wang, Jiankai Sun, Jianping Shi, and Ping Luo. Camnet: Coarse-to-fine retrieval for camera re-localization. In *Int. Conf. Comput. Vis.*, pages 2871–2880, 2019. 3
- [18] Alexey Dosovitskiy and Thomas Brox. Generating images with perceptual similarity metrics based on deep networks. *NeurIPS*, 29:658–666, 2016. 2, 3
- [19] Alexey Dosovitskiy and Thomas Brox. Inverting visual representations with convolutional networks. In *IEEE Conf. Comput. Vis. Pattern Recog.*, pages 4829–4837, 2016. 2, 3
- [20] Mihai Dusmanu, Ondrej Miksik, Johannes L Schonberger, and Marc Pollefeys. Cross-descriptor visual localization and mapping. In *IEEE Conf. Comput. Vis. Pattern Recog.*, pages 6058–6067, 2021. 2, 3, 8
- [21] Mihai Dusmanu, Ignacio Rocco, Tomas Pajdla, Marc Pollefeys, Josef Sivic, Akihiko Torii, and Torsten Sattler. D2-Net: A Trainable CNN for Joint Detection and Description of Local Features. In *IEEE Conf. Comput. Vis. Pattern Recog.*, 2019. 1, 2, 3, 14
- [22] Mihai Dusmanu, Johannes L Schönberger, Sudipta N Sinha, and Marc Pollefeys. Privacy-preserving image features via adversarial affine subspace embeddings. *IEEE Conf. Comput. Vis. Pattern Recog.*, 2020. 2, 3
- [23] Martin A Fischler and Robert C Bolles. Random sample consensus: a paradigm for model fitting with applications to image analysis and automated cartography. *CACM*, 24(6):381–395, 1981. 16
- [24] Xiao-Shan Gao, Xiao-Rong Hou, Jianliang Tang, and Hang-Fei Cheng. Complete solution classification for the perspective-three-point problem. *IEEE Transactions on Pattern Analysis and Machine Intelligence*, 25(8):930–943, 2003. 2, 3, 16
- [25] Marcel Geppert, Viktor Larsson, Pablo Speciale, Johannes L Schönberger, and Marc Pollefeys. Privacy preserving structure-from-motion. In *Eur. Conf. Comput. Vis.*, pages 333–350. Springer, 2020. 2
- [26] Marcel Geppert, Viktor Larsson, Pablo Speciale, Johannes L Schonberger, and Marc Pollefeys. Privacy preserving localization and mapping from uncalibrated cameras. In *IEEE Conf. Comput. Vis. Pattern Recog.*, pages 1809–1819, 2021. 2
- [27] Hugo Germain, Guillaume Bourmaud, and Vincent Lepetit. S2dnet: Learning accurate correspondences for sparse-to-dense feature matching. *Eur. Conf. Comput. Vis.*, 2020. 1, 2, 3
- [28] Shengyu Huang, Zan Gojcic, Mikhail Usvyatsov, Andreas Wieser, and Konrad Schindler. Predator: Registration of 3d point clouds with low overlap. In *Proceedings of the IEEE/CVF Conference on Computer Vision and Pattern Recognition (CVPR)*, pages 4267–4276, June 2021. 4, 13

- [29] Tong Ke and Stergios I. Roumeliotis. An efficient algebraic solution to the perspective-three-point problem. In *Proceedings of the IEEE Conference on Computer Vision and Pattern Recognition (CVPR)*, July 2017. 3, 6
- [30] Alex Kendall and Roberto Cipolla. Modelling uncertainty in deep learning for camera relocalization. In *IEEE Int. Conf. Robot. Autom.*, 2016. 3
- [31] Alex Kendall and Roberto Cipolla. Geometric Loss Functions for Camera Pose Regression With Deep Learning. In *IEEE Conf. Comput. Vis. Pattern Recog.*, 2017. 3
- [32] Alex Kendall, Matthew Grimes, and Roberto Cipolla. Posenet: A convolutional network for real-time 6-dof camera relocalization. In *Int. Conf. Comput. Vis.*, 2015. 2, 3, 6, 9, 14
- [33] Diederik P. Kingma and Jimmy Ba. Adam: A method for stochastic optimization. In *ICLR (Poster)*, 2015. 15
- [34] Laurent Kneip, Davide Scaramuzza, and Roland Siegwart. A novel parametrization of the perspective-three-point problem for a direct computation of absolute camera position and orientation. In *IEEE Conf. Comput. Vis. Pattern Recog.*, 2011. 2
- [35] Zakaria Laskar, Iaroslav Melekhov, Surya Kalia, and Juho Kannala. Camera Relocalization by Computing Pairwise Relative Poses Using Convolutional Neural Network. In *ICCV Workshops*, 2017. 3
- [36] Xiaotian Li, Shuzhe Wang, Yi Zhao, Jakob Verbeek, and Juho Kannala. Hierarchical scene coordinate classification and regression for visual localization. In *IEEE Conf. Comput. Vis. Pattern Recog.*, pages 11983–11992, 2020. 3
- [37] Yunpeng Li, Noah Snavely, and Daniel P. Huttenlocher. Location recognition using prioritized feature matching. In Kostas Daniilidis, Petros Maragos, and Nikos Paragios, editors, *Computer Vision – ECCV 2010*, pages 791–804, Berlin, Heidelberg, 2010. Springer Berlin Heidelberg. 2
- [38] Zhengqi Li and Noah Snavely. Megadepth: Learning single-view depth prediction from internet photos. In *IEEE Conf. Comput. Vis. Pattern Recog.*, 2018. 6, 7, 14
- [39] David G Lowe. Distinctive image features from scale-invariant keypoints. *IJCV*, 60(2):91–110, 2004. 6, 8, 9, 15, 16
- [40] Zixin Luo, Lei Zhou, Xuyang Bai, Hongkai Chen, Jiahui Zhang, Yao Yao, Shiwei Li, Tian Fang, and Long Quan. Aslfeat: Learning local features of accurate shape and localization. In *IEEE Conf. Comput. Vis. Pattern Recog.*, pages 6589–6598, 2020. 1, 2, 3
- [41] Marcela Mera-Trujillo, Benjamin Smith, and Victor Fragoso. Efficient scene compression for visual-based localization. In *2020 International Conference on 3D Vision (3DV)*, pages 1–10, 2020. 2
- [42] Kwang Moo Yi, Eduard Trulls, Yuki Ono, Vincent Lepetit, Mathieu Salzmann, and Pascal Fua. Learning to find good correspondences. In *IEEE Conf. Comput. Vis. Pattern Recog.*, pages 2666–2674, 2018. 5, 13, 14
- [43] Marius Muja and David G Lowe. Scalable nearest neighbor algorithms for high dimensional data. *PAMI*, 36(11):2227–2240, 2014. 1, 6
- [44] Francesco Pittaluga, Sanjeev J Koppal, Sing Bing Kang, and Sudepta N Sinha. Revealing scenes by inverting structure from motion reconstructions. In *IEEE Conf. Comput. Vis. Pattern Recog.*, pages 145–154, 2019. 2, 3
- [45] Filip Radenović, Giorgos Tolias, and Ondřej Chum. Fine-tuning cnn image retrieval with no human annotation. *TPAM*, 41(7):1655–1668, 2018. 14
- [46] Noha Radwan, Abhinav Valada, and Wolfram Burgard. Vlocnet++: Deep multitask learning for semantic visual localization and odometry. *RA-L*, 3(4):4407–4414, 2018. 3
- [47] Paul-Edouard Sarlin, Cesar Cadena, Roland Siegwart, and Marcin Dymczyk. From coarse to fine: Robust hierarchical localization at large scale. In *IEEE Conf. Comput. Vis. Pattern Recog.*, 2019. 2, 3
- [48] Paul-Edouard Sarlin, Daniel DeTone, Tomasz Malisiewicz, and Andrew Rabinovich. Superglue: Learning feature matching with graph neural networks. In *IEEE Conf. Comput. Vis. Pattern Recog.*, pages 4938–4947, 2020. 1, 2, 3, 16
- [49] Paul-Edouard Sarlin, Ajaykumar Unagar, Mans Larsson, Hugo Germain, Carl Toft, Viktor Larsson, Marc Pollefeys, Vincent Lepetit, Lars Hammarstrand, Fredrik Kahl, et al. Back to the feature: Learning robust camera localization from pixels to pose. In *IEEE Conf. Comput. Vis. Pattern Recog.*, pages 3247–3257, 2021. 2, 6, 7, 15, 16
- [50] Torsten Sattler, Bastian Leibe, and Leif Kobbelt. Efficient & Effective Prioritized Matching for Large-Scale Image-Based Localization. *PAMI*, 39(9):1744–1756, 2017. 2, 9
- [51] Torsten Sattler, Will Maddern, Carl Toft, Akihiko Torii, Lars Hammarstrand, Erik Stenborg, Daniel Safari, Masatoshi Okutomi, Marc Pollefeys, Josef Sivic, et al. Benchmarking 6dof outdoor visual localization in changing conditions. In *IEEE Conf. Comput. Vis. Pattern Recog.*, pages 8601–8610, 2018. 1, 2
- [52] Torsten Sattler, Akihiko Torii, Josef Sivic, Marc Pollefeys, Hajime Taira, Masatoshi Okutomi, and Tomas Pajdla. Are Large-Scale 3D Models Really Necessary for Accurate Visual Localization? In *IEEE Conf. Comput. Vis. Pattern Recog.*, 2017. 1
- [53] Torsten Sattler, Qunjie Zhou, Marc Pollefeys, and Laura Leal-Taixe. Understanding the limitations of cnn-based absolute camera pose regression. In *IEEE Conf. Comput. Vis. Pattern Recog.*, 2019. 3, 6, 7
- [54] Johannes Lutz Schönberger and Jan-Michael Frahm. Structure-from-motion revisited. In *IEEE Conf. Comput. Vis. Pattern Recog.*, 2016. 1
- [55] Johannes L Schönberger, Marc Pollefeys, Andreas Geiger, and Torsten Sattler. Semantic Visual Localization. In *IEEE Conf. Comput. Vis. Pattern Recog.*, 2018. 2
- [56] Johannes L Schönberger, Enliang Zheng, Jan-Michael Frahm, and Marc Pollefeys. Pixelwise view selection for unstructured multi-view stereo. In *Eur. Conf. Comput. Vis.*, pages 501–518. Springer, 2016. 1
- [57] Jamie Shotton, Ben Glocker, Christopher Zach, Shahram Izadi, Antonio Criminisi, and Andrew Fitzgibbon. Scene coordinate regression forests for camera relocalization in rgb-d images. In *IEEE Conf. Comput. Vis. Pattern Recog.*, pages 2930–2937, 2013. 2, 6, 15

- [58] Richard Sinkhorn and Paul Knopp. Concerning nonnegative matrices and doubly stochastic matrices. *PJM*, 21(2):343–348, 1967. 4, 13
- [59] Pablo Speciale, Johannes L Schonberger, Sing Bing Kang, Sudipta N Sinha, and Marc Pollefeys. Privacy preserving image-based localization. In *IEEE Conf. Comput. Vis. Pattern Recog.*, pages 5493–5503, 2019. 2
- [60] Jiaming Sun, Zehong Shen, Yuang Wang, Hujun Bao, and Xiaowei Zhou. Loftr: Detector-free local feature matching with transformers. In *CVPR*, pages 8922–8931, 2021. 6, 16
- [61] Weiwei Sun, Wei Jiang, Eduard Trulls, Andrea Tagliasacchi, and Kwang Moo Yi. Acne: Attentive context normalization for robust permutation-equivariant learning. In *Proceedings of the IEEE/CVF Conference on Computer Vision and Pattern Recognition (CVPR)*, June 2020. 1, 2
- [62] Hajime Taira, Masatoshi Okutomi, Torsten Sattler, Mircea Cimpoi, Marc Pollefeys, Josef Sivic, Tomas Pajdla, and Akihiko Torii. InLoc: Indoor Visual Localization with Dense Matching and View Synthesis. In *IEEE Conf. Comput. Vis. Pattern Recog.*, 2018. 2
- [63] Hugues Thomas, Charles R. Qi, Jean-Emmanuel Deschaud, Beatriz MarcoteGui, Francois Goulette, and Leonidas J. Guibas. Kpconv: Flexible and deformable convolution for point clouds. In *Proceedings of the IEEE/CVF International Conference on Computer Vision (ICCV)*, October 2019. 13
- [64] Carl Toft, Will Maddern, Akihiko Torii, Lars Hammarstrand, Erik Stenborg, Daniel Safari, Masatoshi Okutomi, Marc Pollefeys, Josef Sivic, Tomas Pajdla, et al. Long-term visual localization revisited. *TPAMI*, 2020. 1, 2
- [65] Akihiko Torii, Relja Arandjelovic, Josef Sivic, Masatoshi Okutomi, and Tomas Pajdla. 24/7 place recognition by view synthesis. In *CVPR*, pages 1808–1817, 2015. 6, 14, 15
- [66] Dmitry Ulyanov, Andrea Vedaldi, and Victor Lempitsky. Instance normalization: The missing ingredient for fast stylization, 2017. 13
- [67] Ashish Vaswani, Noam Shazeer, Niki Parmar, Jakob Uszkoreit, Llion Jones, Aidan N Gomez, Łukasz Kaiser, and Illia Polosukhin. Attention is all you need. In I. Guyon, U. V. Luxburg, S. Bengio, H. Wallach, R. Fergus, S. Vishwanathan, and R. Garnett, editors, *Advances in Neural Information Processing Systems*, volume 30. Curran Associates, Inc., 2017. 4, 13
- [68] Florian Walch, Caner Hazirbas, Laura Leal-Taixe, Torsten Sattler, Sebastian Hilsenbeck, and Daniel Cremers. Image-based localization using lstms for structured feature correlation. In *Int. Conf. Comput. Vis.*, 2017. 3
- [69] Qianqian Wang, Xiaowei Zhou, Bharath Hariharan, and Noah Snavely. Learning feature descriptors using camera pose supervision. In *Eur. Conf. Comput. Vis.*, 2020. 1, 2, 3, 6, 8
- [70] Yue Wang, Yongbin Sun, Ziwei Liu, Sanjay E. Sarma, Michael M. Bronstein, and Justin M. Solomon. Dynamic graph cnn for learning on point clouds. *ACM Trans. Graph.*, 38(5), Oct. 2019. 13
- [71] Luwei Yang, Ziqian Bai, Chengzhou Tang, Honghua Li, Yasutaka Furukawa, and Ping Tan. Sanet: Scene agnostic network for camera localization. In *IEEE Conf. Comput. Vis. Pattern Recog.*, pages 42–51, 2019. 3
- [72] Jiahui Zhang, Dawei Sun, Zixin Luo, Anbang Yao, Lei Zhou, Tianwei Shen, Yurong Chen, Long Quan, and Hongen Liao. Learning two-view correspondences and geometry using order-aware network. In *Proceedings of the IEEE/CVF International Conference on Computer Vision (ICCV)*, October 2019. 1
- [73] Qunjie Zhou, Torsten Sattler, Marc Pollefeys, and Laura Leal-Taixe. To learn or not to learn: Visual localization from essential matrices. In *IEEE Int. Conf. Robot. Autom.*, pages 3319–3326. IEEE, 2020. 3

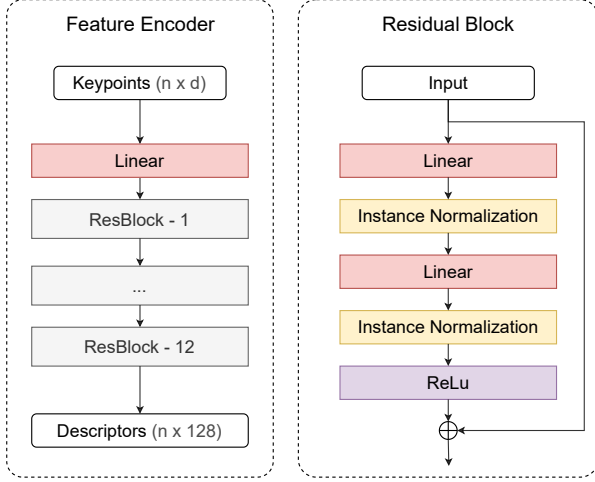


Figure 5. Feature Encoder (left) & Residual Block (right)

In this supplementary material, we provide additional insights and details about certain aspects of the main paper that were not fundamental for its understanding, but that are helpful for interested readers, to fully comprehend and replicate our method. In Appendix A, we provide in-depth descriptions of each network component with mathematical definitions as well as architecture diagrams. Next, we present dataset preparation details including dataset processing, query sampling and correspondence gt generation in Appendix B, followed by the implementation details regarding our training procedure, hyper-parameter choices and an overview of inference process in Appendix C. Finally in Appendix D, we provide additional details on how to compute the metrics used in the paper, in particular the mean reprojection error Area Under the cumulative Curve (AUC). We will release our code upon paper acceptance.

A. Architecture Details.

Feature Encoder. We adopt the same encoder architecture as the one presented in [9, 42], which is shown in Fig. 5. The encoder (*left*) consists of a cascade of residual blocks, where each block (*right*) is composed of sequential point-shared fully connected layers, followed by instance normalization and non-linearity (ReLU). We use two siamese encoders with shared weight parameters to encode bearing vectors of both 2D image keypoints and 3D points, since it has been shown to improve GoMatch’s performance (Section 5.3).

Attention. We use a graph neural network to update features from the same domain (*self-attention*) and multi-head attention layers to exchange features across domains (*cross-attention*). This is similar to PREDATOR [28], although in that work, the attention module is inserted in the bottleneck of the keypoint encoder, *i.e.*, KPConv [63], and thus it is ap-

plied to the downsampled keypoints. In our case, the feature encoder does not have a bottleneck and we instead apply the attention directly to the final output of our encoder. The full attention module contains self \rightarrow cross \rightarrow self-attention layers and is applied to both query and database encoded features.

We employ an independent graph neural network [70] to the features coming from each domain. These exchange and refine features of every keypoint type with a fixed number of closest neighbors in coordinate space. Let $\mathbf{f}_i \in \mathbb{R}^d$ represent the feature for keypoint i and \mathbf{f}_j the feature corresponding to one of its neighbors. Let \mathcal{E}_i represent the set of edges formed between keypoint i to its closest K neighbors in coordinate space. We update feature f_i according to

$$\mathbf{f}_i^{(k+1)} \Big|_{k=\{0,1\}} = \max_{j:(i,j) \in \mathcal{E}_i} h_\theta \left(\text{cat}[\mathbf{f}_i^{(k)}, \mathbf{f}_j^{(k)} - \mathbf{f}_i^{(k)}] \right) \quad (4)$$

$$\mathbf{f}_i^{(3)} = h_\theta \left(\text{cat}[\mathbf{f}_i^{(0)}, \mathbf{f}_i^{(1)}, \mathbf{f}_i^{(2)}] \right), \quad (5)$$

where h_θ is a composition of a fully connected layer, instance normalization [66], and a leaky ReLU, and $\mathbf{f}_i^{(0)}$ is the feature produced by the encoder for keypoint i .

To exchange information across domains we leverage cross-attention [67]. In a cross-attention layer, every keypoint in a domain will interact with keypoints from the other domain through multi-head attention. There are three important concepts that govern this interaction: queries, keys and values. This setup mimics traditional maps or dictionaries, albeit in a continuous form, where every key is paired with a value and these values can be extracted by querying them with the appropriate key. Specifically, given a feature \mathbf{f}_i coming from a keypoint in one domain and features \mathbf{g}_j from an arbitrary keypoint j in the other domain, we form the query, keys and values according to $\mathbf{q}_i = \mathbf{W}_q \mathbf{f}_i$, $\mathbf{k}_j = \mathbf{W}_k \mathbf{g}_j$ and $\mathbf{v}_j = \mathbf{W}_v \mathbf{g}_j$, where $\mathbf{W}_q, \mathbf{W}_k, \mathbf{W}_v \in \mathbb{R}^{d \times d}$ are parameters learned by the network. We update feature \mathbf{f}_i according to

$$\alpha_{ij} = \text{softmax}(\mathbf{q}_i^\top \mathbf{k}_j / \sqrt{d}) \quad (6)$$

$$\mathbf{m}_i = \sum_j \alpha_{ij} \mathbf{v}_j \quad (7)$$

$$\mathbf{f}_i^{(k+1)} = \mathbf{f}_i^{(k)} + \text{MLP}(\text{cat}[\mathbf{q}_i, \mathbf{m}_i]). \quad (8)$$

Sinkhorn matching. After getting refined features from the attention module, the Sinkhorn matching stage is responsible for assigning correspondences between query and database keypoints. To that effect, we leverage the Sinkhorn algorithm [14, 58] that has foundations in optimal transport theory, to solve the assignment problem with holistic reasoning. Sinkhorn produces a joint discrete probability distribution of two keypoints being matched. Consider the fol-

lowing features after attention $\mathbf{f}_i^{\text{ATT}}$ and $\mathbf{g}_j^{\text{ATT}}$, corresponding to the i -th query keypoint and the j -th database keypoint. We construct an assignment cost matrix $\mathbf{M} \in \mathbb{R}^{M \times N}$ as

$$m_{ij} = \left\| \frac{\mathbf{f}_i^{\text{ATT}}}{\|\mathbf{f}_i^{\text{ATT}}\|} - \frac{\mathbf{g}_j^{\text{ATT}}}{\|\mathbf{g}_j^{\text{ATT}}\|} \right\|, \quad (9)$$

where m_{ij} is the element in the i -th row and j -th column of \mathbf{M} . Sinkhorn provides a solution for the following entropy regularized optimization problem:

$$\mathbf{P}^* = \arg \min_{\mathbf{P} \in \mathcal{U}(\mathbf{r}, \mathbf{c})} \sum_{i=1}^M \sum_{j=1}^N m_{ij} p_{ij} - \tau p_{ij} \log p_{ij} \quad (10)$$

where $\mathcal{U}(\mathbf{r}, \mathbf{c}) := \{\mathbf{P} \in \mathbb{R}_+^{M \times N}, \mathbf{P} \mathbf{1}_N = \mathbf{c}, \mathbf{P}^\top \mathbf{1}_M = \mathbf{r}\}$, $\mathbf{r} \in \mathbb{R}_+^M$, $\mathbf{c} \in \mathbb{R}_+^N$, $\sum_i r_i = 1$, $\sum_j c_j = 1$ and with $\mathbf{1}_M$ denoting a vector of 1s of size M . The vectors \mathbf{r} and \mathbf{c} represent the (marginal) probability vectors of keypoints being matched. In our setup, these marginals are initialized uniformly. The hyperparameter $\tau > 0$ controls the strength of the regularization. This problem is solved iteratively and in a differentiable way through successive steps of row and column-wise normalization, as presented in Cuturi [14].

In a realistic scenario, many of these keypoints will not have a match and in the worst case scenario, it can happen that all points from both sets are unmatched. To handle that, we update the matching cost matrix \mathbf{M} with an extra row and column that act as a ‘‘gutter’’ for unmatched points and denote this new matrix $\tilde{\mathbf{M}} \in \mathbb{R}^{M+1 \times N+1}$. We also add an extra element to both row and column marginals, that is able to ‘‘absorb’’ all unmatched points in the other set if needed, forming the augmented marginals $\tilde{\mathbf{r}} \in \mathbb{R}_+^{M+1}$ and $\tilde{\mathbf{c}} \in \mathbb{R}_+^{N+1}$. We present the updated cost matrix and marginals below

$$\tilde{\mathbf{r}} = \begin{bmatrix} \frac{1}{M+N} \\ \vdots \\ \frac{1}{M+N} \end{bmatrix} \begin{bmatrix} m_{11} & \dots & m_{1N} & m_u \\ \vdots & \ddots & \vdots & \vdots \\ m_{M1} & \dots & m_{MN} & m_u \\ m_u & \dots & m_u & m_u \end{bmatrix} = \tilde{\mathbf{M}} \quad (11)$$

$$\begin{bmatrix} \frac{1}{M+N} & \dots & \frac{1}{M+N} & \frac{M}{M+N} \end{bmatrix} = \tilde{\mathbf{c}}, \quad (12)$$

where m_u is a parameter learned by the network that represents the cost of considering points as unmatched. With the cost and marginals as input, Sinkhorn generates the final discrete probability distribution $\tilde{\mathbf{P}} \in \mathbb{R}_+^{M+1 \times N+1}$, representing soft correspondences. The pose estimation pipeline requires hard correspondences so we retain only pairs of keypoints that mutually assign to each other.

Outlier rejection. After Sinkhorn matching, the estimated corresponding pairs may still contain outlier matches. We follow [42] to cast the outlier rejection as a binary classification task, where we use a classifier to predict a confidence

score to identify whether a match is an inlier or outlier w.r.t. a specific confidence threshold. As depicted in Fig. 6, given a predicted match referring to a query keypoint $Query_P_j$ and a database keypoint DB_P_i , we first collect keypoint feature (extracted in the previous stage by the encoder and attention module). We then concatenate the features of its involved keypoints to form a single feature representation of that match and feed it into a classification network. The classifier follows the overall architecture of keypoint encoder described in Fig. 5 and has a final classification layer, *i.e.*, a linear layer and a sigmoid operation, to output a probability score for an input match which is then used to filter a less confident match.

B. Dataset Details.

MegaDepth [38]. Our networks are trained on MegaDepth. We first followed the preprocessing steps from [21] to generate the undistorted reconstructions. We adopted the test set published by MegaDepth’s authors, composed of 53 sequences. We further split the remaining sequences into training and validation splits, where the training and validation splits ensure a similar distribution in terms of sequence sizes between both. Within each data split, we first sample up to 500 queries per scene. For each query, we collect its k co-visible views that have at least 35% of visual overlapping, where we drop queries with not enough co-visible views, *i.e.*, $k < 3$. The visual overlapping is computed by the number of commonly seen 3D points divided by the total seen 3D points in the query view. Notice, in practice, those co-visible views are supposed to be obtained by image retrieval techniques [1, 45, 65] (as we do for evaluating on the other two benchmark datasets). However, for training and ablation study, we use ground-truth information provided by the dataset to guarantee the co-visibility, which enables stable training and allows us to focus on analysing the geometric-based matching performance with proper retrieval quality.

In total, our training set contains 18881 queries covering 99 scenes, our validation set contains 3146 queries covering 16 scenes and our testing set contains samples 7344 covering 49 scenes.

Cambridge Landmarks [32] Cambridge Landmarks is an outdoor urban localization dataset, where each frame is annotated with a camera pose label. The video footage was captured through a smartphone camera and includes significant urban clutter from pedestrian and vehicles. The dataset is composed of five scenes and each scene is composed of multiple sequences. We report results in four of these scenes – King’s College, Old Hospital, Shop Facade and St. Mary’s Church – amounting to a total of 29 sequences, that in our case were all used for testing. To obtain 3D points for our method, we use the publicly available recon-

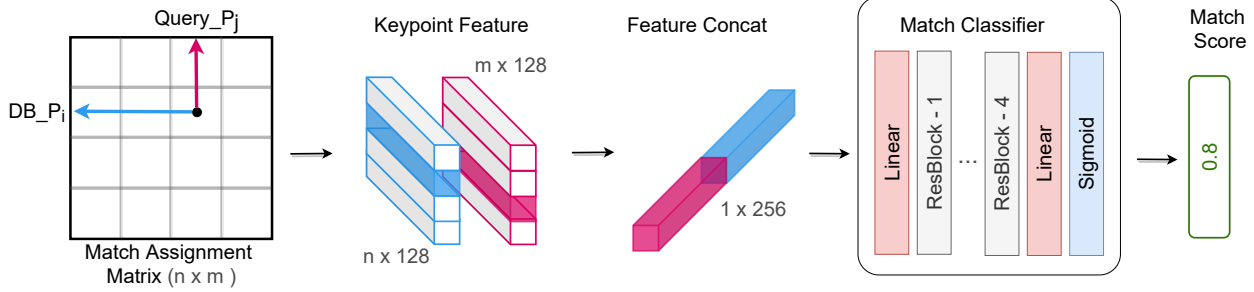


Figure 6. Outlier rejection through classification. For a match identified by Sinkhorn, we collect the matched keypoint features that are extracted by the encoder and attention module. The feature for a query keypoint and a database keypoint is concatenated into a single feature representing the match. The match classifier then predicts the match confidence (as a probability score) which can be used later to filter a less confident match.

struction generated per-scene with SuperPoint [16] from the training images and ground truth poses. This reconstruction was originally made by Torsten Sattler and has been used in the recent work PixLoc [49] for localization evaluation. In addition, we also follow PixLoc to use their released top-10 query-retrieval pairs computed by NetVLAD [1]. Both reconstruction and retrieval pairs are hosted [here](#) by the authors of PixLoc.

7-Scenes [57]. 7-Scenes is a pose annotated indoor dataset of seven different scenes, captured with an RGB-D camera. Each scene is composed of multiple sequences and every frame in each sequence comes with a color image, a depth image, and the camera pose. The dataset has a total of 46 sequences and we used 18 for testing, following the original test split. We use the top-10 query-retrieval pairs computed by DenseVLAD [65] which were made available [here](#) by the authors of PixLoc [49] and used in their experiments. To obtain reference 3D points from database retrievals, we first use a keypoint detector on the color image to generate an original set of candidate 2D keypoints. We then transform their coordinates from the color image space to depth image space and only retain keypoints that have a valid depth measurement, rounding fractional coordinates to the nearest pixel location. Given a 2D image location and the corresponding depth value, we compute a 3D keypoint in camera space and then transform it to scene’s frame of reference. For simplicity and enabled by the fact that we only make use of a sparse subset of points in the original depth image, we don’t try to establish 3D point correspondences between different co-visible frames and consider that each depth image observes a set of unique 3D points in each frame. Such a process allows us to flexibly generate 3D points using different types of keypoint. As shown in Section 5.6, we generated two versions of 3D points that are obtained using SIFT [39] and SuperPoint [15] keypoints to demonstrate the generalization capability of GoMatch.

Keypoint detection. To be consistent with the 3D models in MegaDepth that is reconstructed with SIFT [39] key-

points, we also use SIFT detector to extract keypoints from query images. We limit all detectors to extract up to 1024 keypoints per image, this is to fit our model into a 12GB GPU during testing. On 7-Scenes, we are able to apply any keypoint detectors since we have the depth map that is not limited to a specific type of keypoints. In our experiments, we used a hand-crafted detector – SIFT – and a state-of-the-art learning-based detector – SuperPoint [16] – to extract keypoints. For Cambridge Landmarks, we also used SuperPoint, ensuring consistency with the reconstructed 3D model. All of the keypoints are pre-computed for both datasets and cached locally.

Ground truth correspondences. To train our network with the matching loss and to compute reprojection-based AUC metric (*c.f.* Appendix D), we need to generate ground truth (gt) correspondence labels between query keypoints and 3D point cloud keypoints (database keypoints). Given a set of database keypoints and a query image with its known camera pose, we project the 3D points into the query image to obtain its 2D projections. Then we perform mutual nearest neighbour search based on the L2 distance between the query keypoints and the projected 3D keypoints and consider them as a gt correspondence if the distance is below a threshold of 1px.

C. Implementation Details

Architecture. We used 12 residual blocks for keypoint encoders (*c.f.* Fig. 5) and 4 residual blocks for match classifier for outlier rejection (*c.f.* Fig. 6). The features produced by the keypoint encoders and attention module have dimension 128. The graph neural network used for *self attention* establishes a KNN graph with the closest 10 neighbors, in coordinate space. We use 4 parallel heads for multi-head *cross attention*. In total, GoMatch has approximately 1.3M weight parameters.

Training. We train all models using ADAM [33] optimizer at the learning rate of 0.001. The batch sizes are chosen to

allow each model to be trained on a single 48GB NVIDIA Quadro RTX 8000 GPU and vary from 16 to 64 batches (depending on the model size), *e.g.*, we use batch size 16 for GoMatch. We train each model for 50 epochs and determine the best checkpoint based on the lowest matching loss on the validation set. GoMatch requires approximately 20 hours training time for 50 epochs.

Outlier rate control. The keypoints involved in gt matches are the inlier keypoints and the remaining keypoints are considered outliers. For training stability we constrain the keypoint outlier rate to 0.5. Besides our ablation studies shown in Fig. 4, no keypoint outlier control is applied during testing.

Keypoint number control. By default, we limit query and database keypoints to a maximum number of 1024, to ensure the testing can be performed on a 12GB GPU. For query keypoints, we enforce the detector to extract at most 1024 keypoints. For database keypoints, we use up to its first 1024 keypoints if exceeding that number. During training, we ignore training samples where the number of query keypoints or database keypoints is less than 100. During inference, we consider a sample as failed if the number of query keypoints or database keypoints is less than 10.

Inference. Given a query image and a 3D point cloud, we first extract 2D keypoints from the query using detectors such as SIFT [39] or SuperPoint [16] (in practice, we load pre-computed keypoints). Next, we identify k retrieval/co-visible reference views to compute 3D points that are visible to query. Correspondences are established between the query keypoints and co-visible 3D points (in bearing vectors) by GoMatch. We run the Sinkhorn algorithm for a maximum of 20 iterations to obtain an initial set of match estimates. Then we remove all matches with classification scores below a threshold 0.5 to filter uncertain matches and finally estimate camera pose of the query.

Pose estimation. We use the OpenCV [8] library to estimate pose from a set of query to point cloud keypoint correspondences. We first identify an initial set of inlier matches using a minimal P3P [24] solver paired with RANSAC [23] and then estimate the final pose through a Levenberg-Marquardt optimization step acting only on the inliers. we allow RANSAC to perform 1000 iterations with the admissible maximum inlier error threshold for the bearing vectors set to $1e-3$.

D. Reprojection Error AUC

For MegaDepth, we reported the mean reprojection error area under the cumulative curve (AUC) with thresholds at 1, 5 and 10 pixels. This metric was inspired by the pose error area under the cumulative curve used in [48, 49, 60]. However, in our case, as the scale unit of MegaDepth is

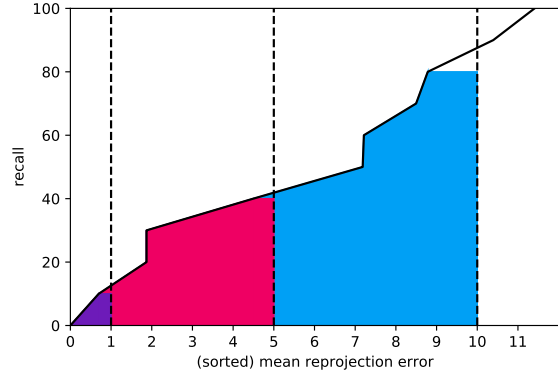


Figure 7. A hypothetical example of how the mean reprojection error AUC is computed for the thresholds at 1/5/10 pixels. After sorting the mean reprojection error and establishing a bijective relation with the recall, one computes the area under the curve using the trapezoidal rule of integration. Despite not visible, the AUC in cyan for the 10 pixel threshold spans from 0 to 10, and similar to the pink area for the 5 pixels threshold.

undetermined and might be inconsistent across scenes, we have to compute the AUC based on reprojection error instead of pose errors for consistency. To compute our proposed AUC metric, for each query, we project the inlier 3D points, *i.e.*, the 3D points involved in the ground-truth (gt) correspondences, onto the query image using the gt pose and the estimated pose. The mean reprojection errors are computed as the means pixel distances between the gt projections and estimated projections of the 3D points. Then we compute the area under the cumulative recall curve up to a specific pixel error threshold as illustrated in Fig. 7. Finally, we normalize the area by the error threshold to keep the metric score $\in [0, 100]$.

As described in Appendix B, the gt correspondences are computed at 1 px threshold, which means the 2D projections obtained by projecting the inlier 3D points using the gt camera pose have up to 1 pixel distances to our labelled gt 2D keypoints. Therefore, this metric produced relatively low scores at 1 pixel threshold (Table 1)) even using our Oracle matcher. However, this does not affect the function of the AUC metric that is to reveal the performance gap between different methods. We showed that the AUC metric yields similar conclusion as the pose error quantile metric used by BPnPNet [9].